ACS APPLIED NANO MATERIALS

www.acsanm.org Article

Triggering Passive Molecular Transport into Cells with a Combination of Inhomogeneous Magnetic Fields and Magnetic Nanoparticles

Wasundara Hulangamuwa, Basanta Acharya, Viktor Chikan,* and Ryan J. Rafferty*

Cite This: *ACS Appl. Nano Mater.* 2020, 3, 2414–2420 Read Online

ABSTRACT: Microporation techniques facilitate the passive transport of molecules into cells via mechanical, electrical, or magnetic simulation. In this work, a combinatorial microporation technique is demonstrated utilizing small superparamagnetic particles and inhomogeneous magnetic pulses. This microporation technique is applied to facilitate the transport of a model therapeutic agent (doxorubicin) into the U937 cancer cell line. This work demonstrates that the drug transport of doxorubicin to the U-937 cancer line increases by 75% when the cells are exposed to only a few inhomogeneous magnetic pulses. The increased transport resulted in more effective destruction of the cancer cells demonstrating that the technique can be utilized to increase the effectiveness of common cancer drugs. The results also demonstrate that the presence of the magnetic particles or the presence of the magnetic fields does not show significant effect on cell viability in the presence of cancer drugs.

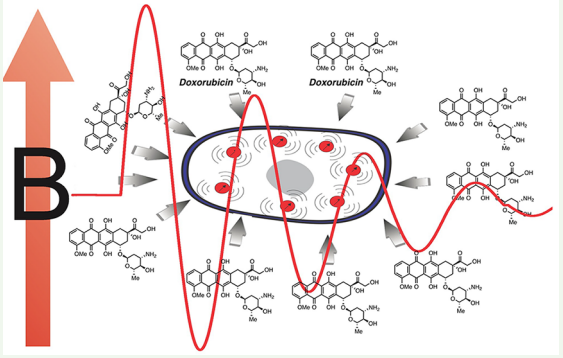

KEYWORDS: *combinatory microportion, transport enhancement, syngergistic strategy, inhomogeneous magnetic fields, Dextrin-IONPs*

INTRODUCTION

Microporation is a methodology that increases passive transport of macromolecules across membranes of living eukaryotic cells.[1] In this, a physical stimulus, such as electrical, magnetic, or mechanical is applied upon a cell that will alter the permeability of the membranes. Microporation techniques are actively used to transport genes, drugs,[2] and cell nutrients[3] to cells that otherwise are not available due to the low passive transport of these molecules. Electroporation techniques subject cells to electric fields to open up pores for drug delivery, achieved by the administration of high voltage electric fields to polarize the cell membrane.[4] Pore formation in this technique requires a membrane potential larger than 200 mV. This technique involves the close contact of an electrode pair for the administration of electric fields. Magnetoporation techniques rely on the application of homogeneous static or pulsed magnetic fields to create pores in the cell membrane.[5] Both electroporation and magnetoporation are based in the polarization of the membrane resulting in irreversible microporation. Sonoporation (cellular sonication) uses sound waves (typically ultrasonic frequencies) to modify the permeability of the cell membrane.[5,6]

EXPERIMENTAL DESIGN

With the aim of enhancing small molecule transport into cells, we propose a combination of inhomogeneous pulsed magnetic fields with magnetic nanoparticles to produce sound waves locally.[7] Magnetic fields are not attenuated the same extent as sound waves, therefore the combination of the magnetic fields and nanoparticles can be used in areas that were not available with pure sonoporation techniques. In addition, the use of magnetic particles with specific ligands enables us to develop molecularly targeted microporation techniques. While both sound waves and magnetic fields affect the cells, their effect is minimal, and it is the interaction of these two aspects that leads to successful microporation of the membrane. The formation of the micropores is critical in this proposed strategy. Our laboratory,[7] as well as others,[8] have demonstrated that magnetic nanoparticles possess oscillations, resulting in sound generation, due to the application of external magnetic pulses. Furthermore, we have determined that the origin of this oscillation is from the translational motion of the magnetic particles in an inhomogeneous magnetic field. Sound, generated in a variety of ways including oscillation, has been reported to open pores within cell membranes. Our research focuses on developing a new strategy to enhance small molecule transport into cells through a combinatory microporation technique based on application of magnetic pulses and magnetic nanoparticles, iron-oxide in this work (IONPs). Herein, we propose that microporation can be induced by nanoparticles within a cell when subjected to pulses of inhomogeneous magnetic fields (Figure 1), resulting in the formation of micropores that can boost the transport of small molecules into

Received: December 19, 2019
Accepted: February 12, 2020
Published: February 12, 2020

https://dx.doi.org/10.1021/acsanm.9b02537
ACS Appl. Nano Mater. 2020, 3, 2414–2420

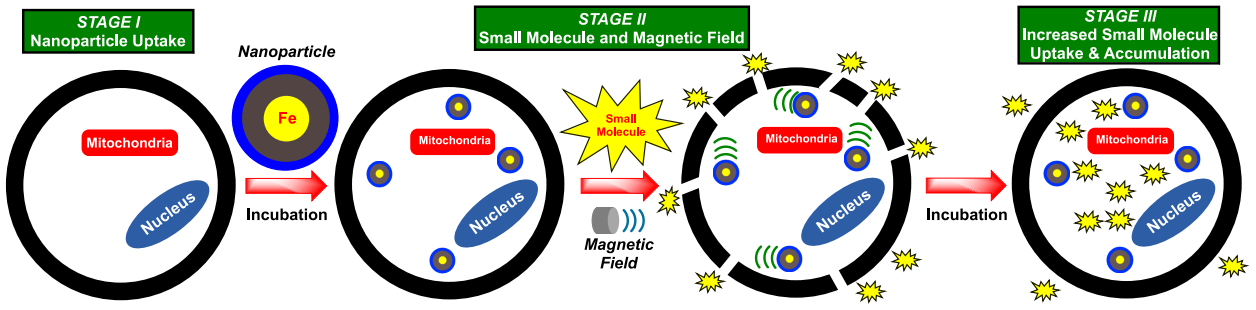

Figure 1. Graphic illustration of the proposed molecule transport via IONPs and the inhomogeneous magnetic field application resulting in small micropore formation for molecule transport.

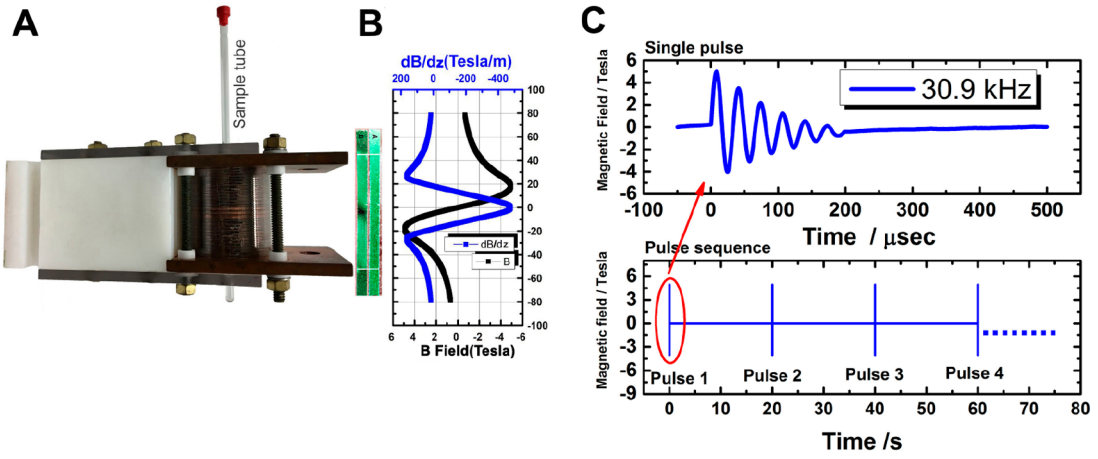

Figure 2. (A) Anti-Helmholtz coil used. (B) Magnetic field/gradient of the coil, and the green magnetic field visualization film illustrating the localization of the inhomogeneous magnetic field before and after application of a magnetic pulse (red box highlights field application). (C) The measured time dependence of the peak magnetic field and graphical illustration of pulse sequence for inhomogeneous magnetic fields.

cells. We envision that this strategy can be universally applied for the transport of small or large molecules into cells; such as, but not limited to anticancer agents and probes.

RESULTS AND DISCUSSION

To investigate this strategy, a pilot study was conducted in which a cell line, small molecule, and means to evaluate the effects of transport were required. As such, we have chosen to use the cancerous lymphocytic leukemia cell lines U-937, anticancer agent doxorubicin, and cellular viability and HPLC as the means to evaluate doxorubicin transport. Converting electromagnetic energy to mechanical energy could be a potentially useful tool to stimulate biological systems for therapeutic purposes when drugs need to be transported into cells. It is well-known that mechanical energy from (ultra)-sound will increase cell permeability,[1] However, its use is somewhat limited due to the loss processes of sound waves in biological media. Alternatively, (ultra)sound waves can be attained from colloidal magnetic nanoparticles in the presence of rapidly changing inhomogeneous magnetic fields.[7] These magnetic fields do not suffer the same attenuation in biological systems as the sound waves;[9] therefore, they could be more effective in many applications. The inhomogeneous magnetic field produces transitional motion on magnetic particles, which leads to pressure fluctuation in a liquid.[10,11] Sound waves generated from magnetic nanoparticles lead to changes of permeability in lipid bilayers resulting in increased transport of small molecules.[12,13] Permeability changes in lipid bilayers due to local heating from magnetic nanoparticles is also possible due to alternating homogeneous magnetic pulses,[14−16] but it is much less likely under the conditions presented in this work.

The magnetic field generator consists of a home-built pulsed power generation system that produces underdamped oscillatory pulsed currents (Figure 2A). The current in the circuit oscillates at an oscillation frequency that corresponds to the resonant frequency of the RLC circuit (30.9 kHz). The inhomogeneous magnetic field is generated from an anti-Helmholtz coil (graph shown in Figure 2B). The localization of the applied field is illustrated within the inset of Figure 2B (magnetic paper which upon magnetic field application shows location of said field), which demonstrates the targeted application possibilities. This arrangement of coil pairs yields magnetic fields that are rapidly changing (Figure 2C) in the center of the coil with respect to the horizontal dimension. The magnetic field generator produces a 200 μs pulse every 20 s. The calculated duty cycle of the magnet is 0.02%. When the fiber optic temperature sensor is placed into the sample tube no detectable temperature rise is observed during the application of inhomogeneous magnetic field pulses (see SI-Figure 1).

The biodistribution, availability, and cellular uptake of iron-oxide nanoparticles (IONPs) have been characterized by numerous research programs.[17−22] Surface modification of the NP coating can translate into further enhanced cellular uptake;[23,24] however, these modifications can alter the relative benign nature of IONPs. Commercially available dextrin coated IONPs (Dex-IONPs, purchased from www.NANOCS.net, MP25-DX-10) were chosen for this project in the aims of

https://dx.doi.org/10.1021/acsanm.9b02537
ACS Appl. Nano Mater. 2020, 3, 2414−2420

maximizing uptake via glucose receptor mediated endocytosis; noting the increased glucose receptor expression upon cancer cells.[25−27] Full characterization of these nanoparticles is available on the manufactures Web site. To investigate the effects of Dex-IONPs in U-937 cells, the comparison of the IC_{50} of doxorubicin in U-937 cells relative to doxorubicin in the presence of various concentrations of the Dex-IONPs (0 to 1×10^{-6} mg/mL, final concentration) was performed. Dex-IONP concentrations higher than 0.01 mg/mL showed IC_{50} values greater relative to the doxorubicin control alone (Table 1). The IONPs themselves have also been reported to interfere with cellular viability assays at high concentrations, such as Alamar blue that was employed in these investigations.[28−30] When Dex-IONPs were employed with dilutions of 1/400 (0.0025 mg/mL), the IC_{50} of doxorubicin returned to normal levels within the margins of standard deviation in both cell density experiments. Additionally, when U-937 cells were grown in the absence or in the presence of Dex-IONPs (0.0025 mg/mL final concentration), there was no difference in cellular viability and growth, within the statistical deviation limits.

Table 1. Assessment of Dextrin Nanoparticle Concentration as a Function of IC_{50} Alteration of Doxorubicin in U-937 (Histiocytic Lymphoma) Human Cancer Cell Line after 48 h Post Dex-IONP Exposure[a]

Dextrin nanoparticle (mg/mL)	Doxorubicin IC_{50}(μM) in U-937, 48 h	
	4000 cells/well, 384 plate, 50 μ L volume	40 000 cells/well, 48 plate, 700 μ L volume
0	0.023 ± 0.012	0.201 ± 0.032
0.25	4.19 ± 0.95	6.25 ± 0.208
0.01	3.44 ± 0.56	4.83 ± 0.028
0.0025	0.018 ± 0.009	0.20 ± 0.019
0.001666	0.018 ± 0.012	0.20 ± 0.027
0.00125	0.022 ± 0.008	0.32 ± 0.022
0.001	0.018 ± 0.014	0.19 ± 0.035
0.0001	0.018 ± 0.011	0.17 ± 0.024
0.000001	0.022 ± 0.019	0.20 ± 0.079

[a]IC_{50} values (μM) as determined by Alamar Blue Quantification. Error is standard deviation of the mean, $n \geq 9$ (triplicate of triplicates); IC_{50} = half maximal inhibitory concentration.

To ensure that the Dex-IONPs were present within the U-937 cells, rather than adsorbed onto the outer membrane of the cells, visualization was performed. U-937 cells were seeded at 40 000 cell/well in 48-well plates, incubated for 24 h in the presence of 0.0025 mg/mL of Dex-IONPs, isolated, and washed with PBS to remove any adhered NPs upon the outer surface of the cells. The cells were fixed by cold methanol, incubated in the presence of Prussian Blue, and then counter stained with Nuclear Fast Red. Visualization was performed under bright field transmission. Prussian Blue stains the iron-oxide core of the Dex-IONPs blue, whereas the Nuclear Fast Red stains cellular membranes.[31−34] In Figure 3 panels A & B, the visualization of U-937 cells in the absence of Dex-IONPs, shows only the effects of the Nuclear Fast Red stain upon the cellular membrane. No blue coloration was observed within their interiors. Figure 3 panels C and D show that when U-937 cells were treated with Dex-IONPs, there was a clear blue coloration within the cells indicating uptake of the NP. It is worth noting the lack of blue coloration on the exteriors of the cellular membranes, highlighted in red by the Nuclear Fast Red stain. Further validation of Dex-IONPs uptake within U-937 was shown by TEM. Figure 3E shows a U-937 cell that was visualized after Dex-IONP incubation (0.0025 mg/mL), the highlighted red box is enlarged in Figure 3F. Within Figure 3F two Dex-IONP clusters are observed. Imaging of just the Dex-IONPs, Figure 3G, shows the same cluster sizes of particles observed in the U-937 cell. The Dex-presence of the IONPs was confirmed by EDX analysis of the area (Figure 3H).

The effects of the Dex-IONPs, doxorubicin, and the application and quantity of magnetic pulses were then investigated. When neither the Dex-IONPs (0.0025 mg/mL) nor doxorubicin (ran at the observed IC_{50} concentration) was present there was no effect upon cell death in the presence of 0, 20, and 50 pulses, as illustrated in Figure 4. With no change in cellular viability in the presence of magnetic pulses, it can be inferred that the inhomogeneous magnetic field alone has no

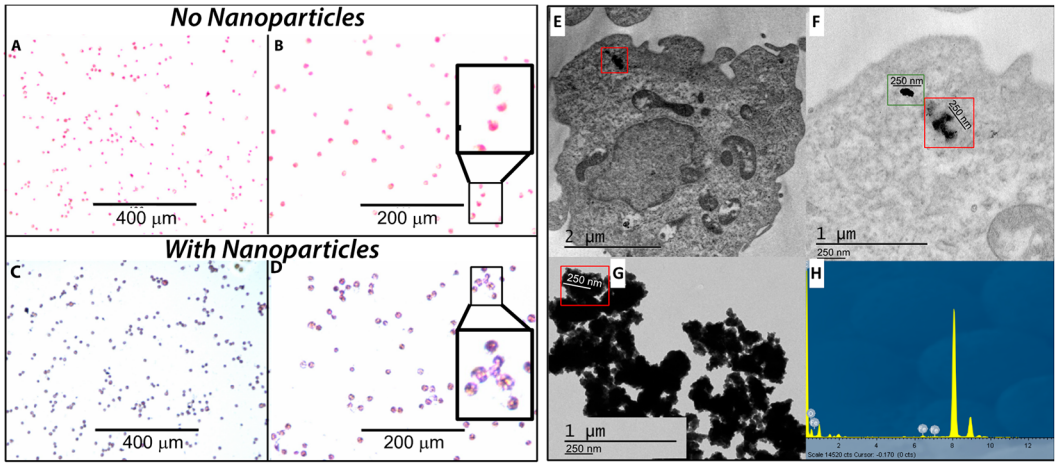

Figure 3. Visualization showing the update of dextrin coated nanoparticles in U-937 human cancer cell line. (A,B) control−absence of nanoparticles; (C,D) uptake; the insets within panels B and D are zoomed in areas for uptake comparison. Scale bars: 400 μm (A,C); 200 μm (B,D). TEM images and spectrum for U-937 cells incubated with Dex-IONPs (E−H): U-937 cell (E), red box enlarged showing two nanoparticle clusters (F). TEM of the Dex-IONPs individually (G), and the spectrum (H). Cells were seeded at 40 000 cells/well in a 48-well plate, incubated with the nanoparticles at a final concentration of 0.0025 mg/mL for 24 h.

https://dx.doi.org/10.1021/acsanm.9b02537
ACS Appl. Nano Mater. 2020, 3, 2414−2420

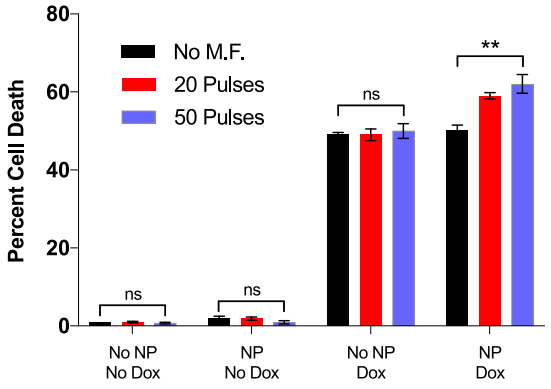

Figure 4. Percentage of U-937 (human cancer cell line) cell death in combinational treatments in the presence or absence of dextrin-coated nanoparticles, doxorubicin, and or 0, 20, or 50 magnetic pulses applied. For each data set: 0.0025 mg mg/mL of dextrin-coated nanoparticles used, 48 h period after magnetic field application. Error is standard deviation of the mean, $n \geq 9$ (triplicate of triplicates): ns = no statistical difference; $^{**}p < 0.01$.

effect upon cell death. The inclusion of Dex-IONPs at 0.025 mg/mL in the absence of doxorubicin with the three-pulse variation showed minimal and statistically nonsignificant increase in cell death relative to the control group. When doxorubicin was introduced, at its observed IC_{50} concentration, in the absence of the Dex-IONPs, cell death increased to ~50% in the presence and absence of magnetic pulses. No increase in cell death was observed when both doxorubicin and Dex-IONPs were present within U-937 with no pulses applied. This result suggests that the presence of the Dex-IONPs, either alone or with doxorubicin in combination, has no increased effect upon cellular viability. However, when 20 pulses were applied, a 15% increase in cell death was observed. Noting that there was no cell death when 20 pulses were applied to the system in which no Dex-IONPs and doxorubicin were present, the 15% increase is correlated to the presence of the magnet field pulses and the effect of said pulses upon the Dex-IONPs, inducing microporation and allowing for an increase influx of doxorubicin. In efforts to increase the observed effects shown with 20 pulses, an increase to 50 pulses was explored (Figure 4, shown in light purple). Direct comparison of the effects of pulses upon cell death in the presence of DOX/IONPs and magnetic fields does show a greater percentage of cell death with higher pulses; Hhowever, a 2.5 increase in pulse application does not result in a 2.5-fold increase in cell death.

While the combinational effects of both the Dex-IONPs and application of the magnetic field did result in an increased cell death response in the presence of doxorubicin, the long-terms of effects of each upon cell viability could not be made. To probe the long-term effects of cells exposed to Dex-IONPs as a function of cell viability, U-937 cells were either treated with Dex-IONPs or an equivalent amount of media only and allowed to incubate for 72 h. No statistical difference was observed between cells treated with various concentration of Dex-IONPs in comparison to cells treated with media only. From this, we can assume that the observed increase in cell death (Figure 3) does not result from long-term exposure of the Dex-IONPs. Treating U-937 cells with 20 pulses of inhomogeneous magnetic fields, and then allowing them to incubate for 72 h show no change in cell viability (Figure 5B). Long-term effects of both Dex-IONPs and 20 magnetic field pulses also show no statistical difference in cellular viability. On the basis of these investigations, we can assume that neither the presence of Dex-IONPs nor the application of magnetic field pulses, either separately or in combination, have any detrimental effects upon U-937 cell viability. As such, we speculate that the observed 15% increase in cell death (Figure 4) is due to the increase transport of doxorubicin into the U-937 cells, and not from the long-term effects of either, or both, the Dex-IONPs and magnetic fields.

To explore if the increased observed cellular death is caused by the increase in doxorubicin uptake, quantification of doxorubicin within U-937 cells was performed in the absence and presence of magnet field pulses. While 50 magnetic field pulses were observed to lead to a marginally higher cellular death compared to 20 pulses, doxorubicin uptake was quantified under the latter conditions. Employing the same experimental conditions used for cellular death analysis, quantification of doxorubicin was achieved via HPLC (method developed, and all relevant chromatograms are presented in the Supporting Information). The protocol of this experiment differed from the cellular death analysis in that quantification of doxorubicin was performed 2 h after magnetic pulse application, rather than 48 h. Rationale for this is based upon the rapid translocation of doxorubicin into the nucleus, in

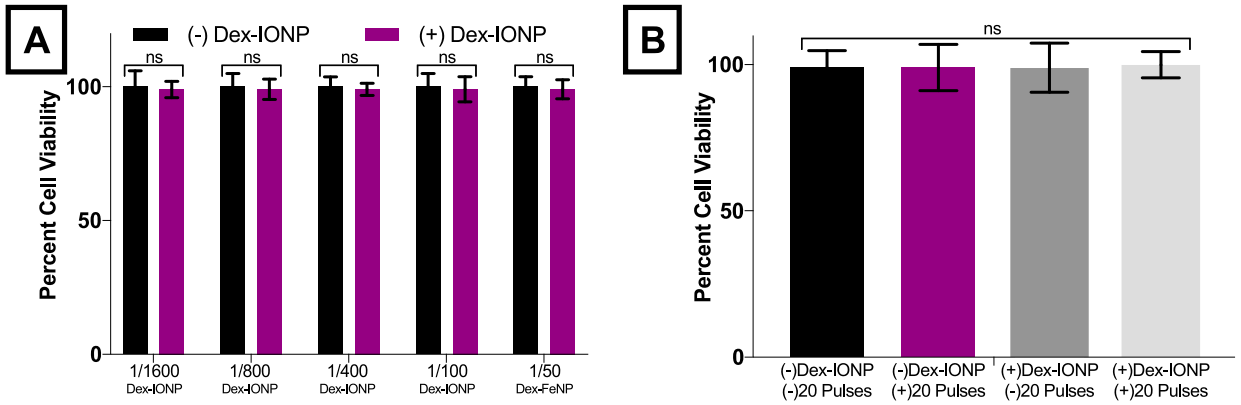

Figure 5. Investigations into the possible individual and combination effects of long-term cell viability of Dex-IONPs (A), and magnetic and combinational application (B) within U-937 cells. (A) Effects upon cell viability with the exposure of various concentrations of Dex-IONPs over a 72-h period. (B) Cell viability effect 72 h after 20 magnetic field pulses applied to U-937 cells and combinational effects of both Dex-IONPs and pulses. Error is relative standard deviation of the mean, $n \geq 9$ (triplicate of triplicates): ns = no statistical difference.

https://dx.doi.org/10.1021/acsanm.9b02537
ACS Appl. Nano Mater. 2020, 3, 2414−2420

which it elicits its therapeutic action. HPLC measurement within U-937 cells in the absence and presence of magnet field pulses showed a 75.2% increase of doxorubicin within cells treated under magnet field pulses relative to those untreated (Figure 6). The quantification of doxorubicin at later time

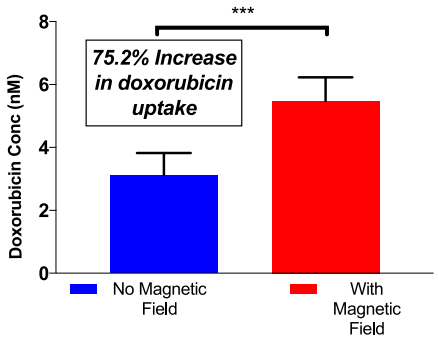

Figure 6. Quantification via HPLC of doxorubicin uptake within U-937 human cancer cells in the presence of 0.0025 mg/mL of dextrin-coated IONPs, 20 magnetic pulses; over 2 h. Error is standard deviation of the mean, $n \geq 9$ (triplicate of triplicates): ns = no statistical difference; ***$p < 0.0001$.

points showed accumulation levels lower than 75% between the two systems. This decrease in free doxorubicin concentrations can be a result of translocation into the nucleus and can be indicative of the initial points of DNA adducts formation. While there are reports that an increase in heat around the cell can translate into higher uptake of agents upon the cell exterior, there is not significant heat generation in this strategy (Supporting Information, Figure SI-1).

With a 15% increase in cellular death as well as a 75% increase in doxorubicin uptake, the next step taken was to investigate the overall drug effectiveness of doxorubicin in this combinational strategy. Doxorubicin was observed to have an IC_{50} of 289 nM in the presence of Dex-IONPs (0.0025 mg/mL), but the IC_{50} dropped to 169 nM when the combinational strategy was applied (Figure 7). This shift in the IC_{50} curve is similar to that of positive potentiators, and in this case results in a near 60% increase in cytotoxicity. Noting that the Dex-IONPs and the application of magnetic field pulses

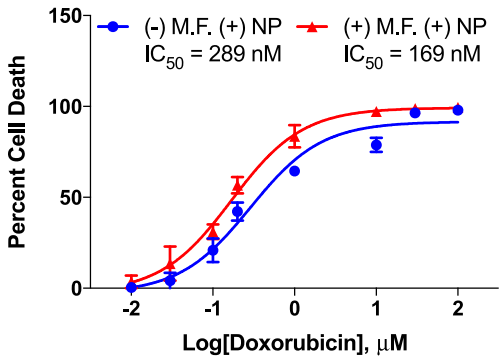

Figure 7. Nanoparticle facilitated by magnetic field effects upon doxorubicin IC_{50} in U-937 human cancer cells. Cells were incubated with nanoparticles at 0.0025 mg/mL for 24 h, drug/blank added along with 20 magnetic pulses applied, incubated for 48 h, and death was determined via the Alamar Blue assay. Cells were plated at 40 000 cells/well in 48 well plate, 48 h. Error is standard deviation of the mean: $n \geq 3$ for each data point.

independently and in combination (Figures 4 and 5) showed no change in cellular viability, this suggests that this combinational strategy in this exploratory investigation is a nontoxic positive potentiating strategy for the increased uptake of desired agents, such as anticancer agents.

CONCLUSIONS

In summary, the application of inhomogeneous magnetic field pulses in the presence of dextrin coated iron-oxide nanoparticles resulting in an increase efficacy of an anticancer agent has been disclosed. Via systematic investigation, each of the three separate components of this combinational strategy was shown to be noneffective independently with regards to increased cellular uptake and increase in cytotoxicity of an anticancer agent. Through employing doxorubicin, a known and currently prescribed anticancer agent, the effects of magnetic field pulses revealed a near 60% increase in doxorubicin's cytotoxicity in U-937 cancer cells that were preincubated with Dextrin-coated nanoparticles. This increase is thought to be caused by near 75% increase in cellular uptake and accumulation of doxorubicin via this combinational strategy. From this pilot study, we propose that through the formation of micropores, induced by oscillation from the magnetic nanoparticles and an applied inhomogeneous magnetic field, transport of doxorubicin into U-937 cells is increased. Further studies are underway to explore multiple effects, such as, but not limited to (1) nanoparticle size and number, (2) optimization of the magnetic field pulse generation, (3) investigations into the application of this strategy in various cancerous (adherent cell lines) and noncancerous cell lines, and (4) employing other anticancer agents and other small molecules to explore the scope of this methods effectiveness.

ASSOCIATED CONTENT

Supporting Information

The Supporting Information is available free of charge at https://pubs.acs.org/doi/10.1021/acsanm.9b02537.

Experimental details, HPLC method development, biological assays performed, and raw data (PDF)

AUTHOR INFORMATION

Corresponding Authors

Viktor Chikan − *Department of Chemistry, Kansas State University, Manhattan, Kansas 66506-0401, United States;* orcid.org/0000-0002-4157-3556; Phone: +1-785-532-6807; Email: vchikan@ksu.edu

Ryan J. Rafferty − *Department of Chemistry, Kansas State University, Manhattan, Kansas 66506-0401, United States;* orcid.org/0000-0002-4835-6343; Phone: +1-785-532-6624; Email: rjraff@ksu.edu

Authors

Wasundara Hulangamuwa − *Department of Chemistry, Kansas State University, Manhattan, Kansas 66506-0401, United States*

Basanta Acharya − *Department of Chemistry, Kansas State University, Manhattan, Kansas 66506-0401, United States*

Complete contact information is available at: https://pubs.acs.org/10.1021/acsanm.9b02537

https://dx.doi.org/10.1021/acsanm.9b02537
ACS Appl. Nano Mater. 2020, 3, 2414−2420

Notes

The authors declare no competing financial interest.

■ ACKNOWLEDGMENTS

This work could not have been undertaken without the gracious financial support of numerous organizations: Johnson Cancer Center of Kansas State University (V.C. and R.J.R.), Startup Capital from Kansas State University to R.J.R., and the NSF (CHE-1608344 to V.C. and CHE-1848186 to R.J.R.).

■ REFERENCES

(1) Sundaram, J.; Mellein, B. R.; Mitragotri, S. An Experimental and Theoretical Analysis of Ultrasound-Induced Permeabilization of Cell Membranes. *Biophys. J.* **2003**, *84* (5), 3087−3101.

(2) Escoffre, J. M.; Mannaris, C.; Geers, B.; Novell, A.; Lentacker, I.; Averkiou, M.; Bouakaz, A. Doxorubicin liposome-loaded microbubbles for contrast imaging and ultrasound-triggered drug delivery. *IEEE Transactions on Ultrasonics, Ferroelectrics, and Frequency Control* **2013**, *60* (1), 78−87.

(3) Singh, T. R.; Garland, M. J.; Cassidy, C. M.; Migalska, K.; Demir, Y. K.; Abdelghany, S. M.; Ryan, E.; Woolfson, A. D.; Donnelly, R. F. Microporation techniques for enhanced delivery of therapeutic agents. *Recent Pat. Drug Delivery Formulation* **2010**, *41*, 1−17.

(4) Weaver, J. C.; Chizmadzhev, Y. A. Theory of electroporation: a review. *Bioelectrochem. Bioenerg.* **1996**, *41* (2), 135−160.

(5) Novickij, V.; Grainys, A.; Novickij, J.; Markovskaja, S. Irreversible magnetoporation of micro-organisms in high pulsed magnetic fields. *IET Nanobiotechnol.* **2014**, *8* (3), 157−162.

(6) Nomikou, N.; McHale, A. P. Exploiting ultrasound-mediated effects in delivering targeted, site-specific cancer therapy. *Cancer Lett.* **2010**, *296* (2), 133−143.

(7) Podaru, G. V.; Chikan, V.; Prakash, P. Magnetic Field Induced Ultrasound from Colloidal Superparamagnetic Nanoparticles. *J. Phys. Chem. C* **2016**, *120* (4), 2386−2391.

(8) Carrey, J.; Connord, V.; Respaud, M. Ultrasound generation and high-frequency motion of magnetic nanoparticles in an alternating magnetic field: toward intracellular ultrasound therapy? *Appl. Phys. Lett.* **2013**, *102* (23), 232404.

(9) Duck, F. A., Chapter 4—Acoustic Properties of Tissue at Ultrasonic Frequencies. In *Physical Properties of Tissues*; Academic Press: London, 1990; pp 73−135.

(10) Kaczmarek, K.; Hornowski, T.; Antal, I.; Timko, M.; Józefczak, A. Magneto-ultrasonic heating with nanoparticles. *J. Magn. Magn. Mater.* **2019**, *474*, 400−405.

(11) Huang, K.-W.; Chieh, J.-J.; Yeh, C.-K.; Liao, S.-H.; Lee, Y.-Y.; Hsiao, P.-Y.; Wei, W.-C.; Yang, H.-C.; Horng, H.-E. Ultrasound-induced magnetic imaging of tumors targeted by biofunctional magnetic nanoparticles. *ACS Nano* **2017**, *11* (3), 3030−3037.

(12) Podaru, G.; Ogden, S.; Baxter, A.; Shrestha, T.; Ren, S.; Thapa, P.; Dani, R. K.; Wang, H.; Basel, M. T.; Prakash, P.; Bossmann, S. H.; Chikan, V. Pulsed Magnetic Field Induced Fast Drug Release from Magneto Liposomes via Ultrasound Generation. *J. Phys. Chem. B* **2014**, *118* (40), 11715−11722.

(13) Wood, A. K.; Sehgal, C. M. A review of low-intensity ultrasound for cancer therapy. *Ultrasound in medicine & biology* **2015**, *41* (4), 905−928.

(14) Nappini, S.; Al Kayal, T.; Berti, D.; Nordèn, B.; Baglioni, P. Magnetically Triggered Release From Giant Unilamellar Vesicles: Visualization By Means Of Confocal Microscopy. *J. Phys. Chem. Lett.* **2011**, *2* (7), 713−718.

(15) Shirmardi Shaghasemi, B.; Virk, M. M.; Reimhult, E. Optimization of Magneto-thermally Controlled Release Kinetics by Tuning of Magnetoliposome Composition and Structure. *Sci. Rep.* **2017**, *7* (1), 7474.

(16) Chen, Y.; Bose, A.; Bothun, G. D. Controlled Release from Bilayer-Decorated Magnetoliposomes via Electromagnetic Heating. *ACS Nano* **2010**, *4* (6), 3215−3221.

(17) Huang, J.; Bu, L.; Xie, J.; Chen, K.; Cheng, Z.; Li, X.; Chen, X. Effects of nanoparticle size on cellular uptake and liver MRI with polyvinylpyrrolidone-coated iron oxide nanoparticles. *ACS Nano* **2010**, *4* (12), 7151−7160.

(18) Chung, T.-H.; Wu, S.-H.; Yao, M.; Lu, C.-W.; Lin, Y.-S.; Hung, Y.; Mou, C.-Y.; Chen, Y.-C.; Huang, D.-M. The effect of surface charge on the uptake and biological function of mesoporous silica nanoparticles in 3T3-L1 cells and human mesenchymal stem cells. *Biomaterials* **2007**, *28* (19), 2959−2966.

(19) Petri-Fink, A.; Chastellain, M.; Juillerat-Jeanneret, L.; Ferrari, A.; Hofmann, H. Development of functionalized superparamagnetic iron oxide nanoparticles for interaction with human cancer cells. *Biomaterials* **2005**, *26* (15), 2685−2694.

(20) Fröhlich, E. The role of surface charge in cellular uptake and cytotoxicity of medical nanoparticles. *Int. J. Nanomed.* **2012**, *7*, 5577.

(21) Sonvico, F.; Mornet, S.; Vasseur, S.; Dubernet, C.; Jaillard, D.; Degrouard, J.; Hoebeke, J.; Duguet, E.; Colombo, P.; Couvreur, P. Folate-conjugated iron oxide nanoparticles for solid tumor targeting as potential specific magnetic hyperthermia mediators: synthesis, physicochemical characterization, and in vitro experiments. *Bioconjugate Chem.* **2005**, *16* (5), 1181−1188.

(22) Laurent, S.; Forge, D.; Port, M.; Roch, A.; Robic, C.; Vander Elst, L.; Muller, R. N. Magnetic iron oxide nanoparticles: synthesis, stabilization, vectorization, physicochemical characterizations, and biological applications. *Chem. Rev.* **2008**, *108* (6), 2064−2110.

(23) Zhang, Y.; Yang, M.; Park, J. H.; Singelyn, J.; Ma, H.; Sailor, M. J.; Ruoslahti, E.; Ozkan, M.; Ozkan, C. A Surface-Charge Study on Cellular-Uptake Behavior of F3-Peptide-Conjugated Iron Oxide Nanoparticles. *Small* **2009**, *5* (17), 1990−1996.

(24) Krais, A.; Wortmann, L.; Hermanns, L.; Feliu, N.; Vahter, M.; Stucky, S.; Mathur, S.; Fadeel, B. Targeted uptake of folic acid-functionalized iron oxide nanoparticles by ovarian cancer cells in the presence but not in the absence of serum. *Nanomedicine* **2014**, *10* (7), 1421−1431.

(25) Younes, M.; Lechago, L. V.; Somoano, J. R.; Mosharaf, M.; Lechago, J. Wide expression of the human erythrocyte glucose transporter Glut1 in human cancers. *Cancer research* **1996**, *56* (5), 1164−1167.

(26) Macheda, M. L.; Rogers, S.; Best, J. D. Molecular and cellular regulation of glucose transporter (GLUT) proteins in cancer. *J. Cell. Physiol.* **2005**, *202* (3), 654−662.

(27) Barron, C. C.; Bilan, P. J.; Tsakiridis, T.; Tsiani, E. Facilitative glucose transporters: implications for cancer detection, prognosis and treatment. *Metab., Clin. Exp.* **2016**, *65* (2), 124−139.

(28) Ong, K. J.; MacCormack, T. J.; Clark, R. J.; Ede, J. D.; Ortega, V. A.; Felix, L. C.; Dang, M. K. M.; Ma, G.; Fenniri, H.; Veinot, J. G. C.; Goss, G. G. Widespread nanoparticle-assay interference: implications for nanotoxicity testing. *PLoS One* **2014**, *9* (3), No. e90650-e90650.

(29) Costa, C.; Brandão, F.; Bessa, M. J.; Costa, S.; Valdiglesias, V.; Kiliç, G.; Fernández-Bertólez, N.; Quaresma, P.; Pereira, E.; Pásaro, E.; et al. In vitro cytotoxicity of superparamagnetic iron oxide nanoparticles on neuronal and glial cells. Evaluation of nanoparticle interference with viability tests. *J. Appl. Toxicol.* **2016**, *36* (3), 361−372.

(30) Griffiths, S. M.; Singh, N.; Jenkins, G. J. S.; Williams, P. M.; Orbaek, A. W.; Barron, A. R.; Wright, C. J.; Doak, S. H. Dextran Coated Ultrafine Superparamagnetic Iron Oxide Nanoparticles: Compatibility with Common Fluorometric and Colorimetric Dyes. *Anal. Chem.* **2011**, *83* (10), 3778−3785.

(31) Rowatt, K.; Burns, R. E.; Frasca, S., Jr; Long, D. M. A combination Prussian blue-hematoxylin and eosin staining technique for identification of iron and other histological features. *J. Histotechnol.* **2018**, *41* (1), 29−34.

(32) Scharlach, C.; Kratz, H.; Wiekhorst, F.; Warmuth, C.; Schnorr, J.; Genter, G.; Ebert, M.; Mueller, S.; Schellenberger, E. Synthesis of acid-stabilized iron oxide nanoparticles and comparison for targeting atherosclerotic plaques: evaluation by MRI, quantitative MPS, and

https://dx.doi.org/10.1021/acsanm.9b02537
ACS Appl. Nano Mater. 2020, 3, 2414−2420

TEM alternative to ambiguous Prussian blue iron staining. *Nanomedicine* **2015**, *11* (5), 1085−1095.
(33) Calero, M.; Chiappi, M.; Lazaro-Carrillo, A.; Rodríguez, M. J.; Chichón, F. J.; Crosbie-Staunton, K.; Prina-Mello, A.; Volkov, Y.; Villanueva, A.; Carrascosa, J. L. Characterization of interaction of magnetic nanoparticles with breast cancer cells. *J. Nanobiotechnol.* **2015**, *13* (1), 16.
(34) Dadashzadeh, E. R.; Hobson, M.; Henry Bryant, L., Jr.; Dean, D. D.; Frank, J. A. Rapid spectrophotometric technique for quantifying iron in cells labeled with superparamagnetic iron oxide nanoparticles: potential translation to the clinic. *Contrast Media Mol. Imaging* **2013**, *8* (1), 50−56.

https://dx.doi.org/10.1021/acsanm.9b02537
ACS Appl. Nano Mater. 2020, 3, 2414−2420